CVD-synthesis of detector quality diamond for radiation hardness detectors of ionizing radiation

© A.V. Krasilnikov,[1] N.B. Rodionov,[1] A.P. Bolshakov,[2] V.G. Ralchenko,[2] S.K. Vartapetov,[3]
Yu.E. Sizov,[3] S.A. Meschaninov,[1] A.G. Meschaninov,[1] V.P. Rodionova,[1] V.N. Amosov,[1]
P.A. Khmelnitsky,[1] A.N. Kirichenko[1]

[1] Institution „Project Center ITER", Moscow , Russia
[2] Prokhorov General Physics Institute of the Russian Academy of Sciences, Moscow, Russia
[3] Optosystems Ltd., Troitsk, Moscow, Russia
e-mail: a.krasilnikov@iterrf.ru

An advanced microwave plasma reactor ARDIS 300 was used to synthesize homoepitaxial structures of monocrystal diamond films at Project Center ITER. High-quality epitaxial diamond films were grown on boron-doped monocrystal diamond substrates using microwave plasma-assisted chemical vapor deposition from methane-hydrogen mixture. Structural and impurity perfection of diamond films were characterized by Raman spectroscopy, photoluminescence, and optical absorption. Prototypes of radiation detectors were created on the basis of grown diamond films with thickness $70-80\,\mu$m,. The p-type substrate with boron concentration ~ 100 ppm served as an electrical contact. Detectors were irradiated by 5.5 MeV particles and 14.7 MeV neutrons, corresponding pulse height spectra were measured and detector sensitivities were determined. Charge collection efficiency for synthesized diamond was shown to achieve 94% and 91% when ~ 4 V/μm electric field applied.

Keywords: diamond films, epitaxy, diamond detector

Introduction

The unique electrophysical properties of diamond as a semiconductor with a bandgap of 5.45 eV [1] (high mobilities (up to $\sim 4000\,\mathrm{cm^2/(V \cdot s)}$) and drift velocity ($\sim 10^7$ cm/s) of charge carriers [2], high dielectric breakdown field, record-high thermal conductivity (up to 24 (W/cm · K)), wide operating temperature range (up to 700°C), high radiation resistance [3–5], and high (up to 100% under certain conditions) efficiency of carrier collection) provide an opportunity to design radiation-hardened ionization radiation detectors [6] and other high-load diamond electronic modules to be applied in high-energy physics, in certain branches of industry utilizing nuclear technology, and in research into thermonuclear plasma [7–14]. In a detector structure, diamond is a solid-state ionization chamber with charge collection at electrodes positioned on both sides of a diamond plate. Shaped by the nuclear reactions in diamond, the amplitude spectrum of a diamond detector within a flux of fast neutrons produced in the synthesis of deuterium and tritium [15] ensured efficient application of diamond detectors in spectrometry of DT neutrons in thermonuclear research at TFTR [7], JT-60U, JET [9], and several other facilities utilizing nuclear technology.

The best characteristics of detectors are achieved when single-crystalline plates and films grown in methane–hydrogen mixtures in microwave plasma reactors are used. The chemical vapor deposition (CVD) technology ensures a low density of impurities (primarily nitrogen) and a relatively high degree of crystalline perfection [16–19].

The most significant progress in synthesis of diamonds with an almost complete charge collection (charge collection efficiency, CCE) under irradiation with alpha particles with an energy of ~ 5.5 MeV has been achieved in the last 20 years in research carried out at Element Six (CCE $= 95-100\%$, energy resolution $\Delta E/E = 0.4-1.2\%$ at plate thickness $\Delta = 100-500\,\mu$m [20,21]); the Tor Vergata University of Rome (CCE $\sim 100\%$ and $\Delta E/E = 1.1\%$, $\Delta = 110\,\mu$m [22]); IIa Technology, Singapore (CCE $\sim 100\%$ and $\Delta E/E = 0.8\%$, $\Delta = 890\,\mu$m [23]); the Hokkaido University and AIST, Japan (CCE $\sim 100\%$ and $\Delta E/E = 0.38\%$, $\Delta = 70-150\,\mu$m [24]); and FSBI TISNCM, Troitsk, Russia ($\Delta E/E = 0.56\%$, $\Delta \sim 100\,\mu$m [25,26]).

The typical thickness of diamond plates in detectors is $200-500\,\mu$m. This thickness should not be smaller than the charge collection distance (CCD). Since the drift velocity of current carriers in diamond starts saturating in electric fields on the order of 1 V/μm, the required bias voltage value may be reduced significantly by making the detector as thin as several tens of micrometers. This explains the appeal of designs based on thin films. One of the methods of fabrication of a thin-film diamond detector involves the epitaxial deposition of undoped diamond by CVD onto a conducting single-crystalline diamond substrate doped with boron [7,27–29]. This p-type substrate is used for epitaxy of the undoped material and as the back contact of a detector,

and the nominally undoped epitaxial diamond layer serves as an active layer of the structure within which the electric field is concentrated and the charge carriers (produced by an ionizing particle) move. Alternatively, a buried graphitized layer produced by ion implantation [30] may serve as the back contact.

in the present study, the results of the first experiments at Project Center ITER on synthesis of homoepitaxial CVD diamond films with a thickness of several tens of micrometers on HPHT (high pressure high temperature) substrates heavily doped with boron (p-type) are reported. The efficiencies of charge collection in synthesized films and their alpha- and neutron-detecting efficiency are examined.

1. CVD synthesis of single-crystalline diamond films

Epitaxial single-crystalline undoped diamond films were grown in an ARDIS-300 microwave plasma reactor (frequency: 2.45 GHz, power: up to 6 kW) produced by Optosystems Ltd. [30]. This reactor was modernized with the specific purpose of synthesis of detector-grade diamond.

The updated reactor design differs from the base model in that leakage into the chamber from the atmosphere is reduced. The concentration of the background nitrogen impurity in the gas mixture is reduced accordingly, thus providing an opportunity to synthesize diamond materials with complete charge collection.

The modernized ARDIS-300 reactor complex allows one to adjust directly the following parameters in the process of synthesis of diamond films: independent inflow of hydrogen, methane, nitrogen, oxygen, and a boron-containing gas or (in future) a boron-containing liquid vapor into the chamber; pressure of the gas mixture in it; microwave radiation power; and vertical position of the substrate. These parameters affect the concentration of the above-mentioned gases in the mixture, the substrate temperature, and, consequently, the growth rate of a diamond film. The pressure in the chamber is maintained by a spiral dry pump, and high vacuum is achieved using a turbomolecular pump. The attainable vacuum value in the reactor is $5 \cdot 10^{-7}$ Torr. Two types of sensors are used to monitor the pressure in the chamber: a Pirani sensor and a capacitance sensor.

High-purity oxygen (99.99999% pure) and methane (99.9999%) were used as reagents. The substrate temperature in the course of synthesis was measured with a Sensortherm Metis M3 two-color IR pyrometer.

The leakage from the atmosphere into the reactor did not exceed $2.5 \cdot 10^{-6}$ Torr · l/s. In the CVD process, this translates into a concentration of N_2 nitrogen molecules of about 2 ppm in the gas mixture in a chamber with a volume of 5 l. The N/C ratio at a typical methane concentration (4%) was ~ 100 ppm. Since the coefficient of incorporation of nitrogen atoms $(N/C)_{dia}/(N/C)_{gas}$ into a growing diamond in the CVD process is $\sim 2 \cdot 10^{-4}$ [31,32], a concentration of nitrogen in the epitaxial material at the level of 20 ppb is to

Table 1. Film synthesis conditions: pressure p, methane concentration in gas [CH$_4$], substrate temperature T_s, microwave power P_{MW}, deposition time t_g, growth rate GR, film thickness d

№ of sample	p, Torr	[CH$_4$] %	T_s, °C	P_{MW}, W	t_g, h	GR, μm/h	d, μm
B21	170	4	940	5500	23.5	3.0	70
B22	170	4	940	5500	23.5	3.2	75
B23	170	4	965	3600	20.0	4.0	80
H03	140	1.5	1050	3500	66	< 1.0	51

be expected (the contribution to the nitrogen concentration in diamond from impurities in the working gas is two orders of magnitude lower, ~ 0.1 ppb).

Conducting diamond plates doped with boron (B21, B22, B23) synthesized in HPHT (high pressure high temperature) reactors were used substrates for epitaxy. The boron concentration was ≈ 100 ppm (in diamond, 1 ppm $= 1.76 \cdot 10^{17}$ cm^{-3}). One film was grown on an undoped HPHT substrate (H03) with a low nitrogen concentration (type IIa) in order to determine the concentration of single substituent nitrogen atoms in a neutral charge state (N_s^0), which are traditionally called C defects, in the grown epitaxial material. The conditions of H03 film synthesis were the same as those set for samples B21−B23.

Polished substrates were $4.5 \times 4.5 \times 0.5$ mm in size with (100) growth faces. The surface roughness measured with a Solver Next (NT-MDT) atomic force microscope did not exceed 5 nm. The results of measurements with a Bruker D8 Discover A25 DaVinsiDesign X-ray diffractometer revealed that the deviation of orientation of the working face of selected substrates from crystallographic plane (100) did not exceed 3 degrees. Prior to loading into the reactor chamber, substrates were annealed in a muffle furnace in air at a temperature of 590°C to remove the non-diamond carbon phase, boiled in a solution of potassium bichromate ($K_2Cr_2O_7$) in concentrated sulphuric acid (H_2SO_4) to remove the possible surface contaminants after polishing, and treated with isopropyl alcohol in an ultrasonic bath. The growth conditions are detailed in Table 1. Diamond layers with a thickness of 50–80 μm were produced as a result. The growth rate of film B23 was higher due to the fact that the substrate was positioned higher (closer to plasma).

Nomarski differential interference contrast (DIC) microscopy was used to examine the surfaces of synthesized samples with an Olympus BX43 optical microscope. Film B21 had a relatively smooth layer growth surface; hillock-type macrodefects, which are often observed in CVD diamond synthesis [33], were lacking. The surface of film B22 is more developed: it features a certain number of hillocks and a polycrystalline film on side faces. Sample B23 has lots of hillocks distributed over the entire surface. The morphology of film B21 was rated as the best in the series.
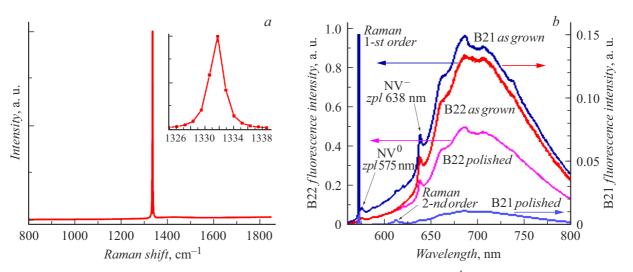
Figure 1. *a* — Raman spectrum of sample B21. The Raman spectrum in the $1320-1340\,\text{cm}^{-1}$ range is shown in the inset; *b* — PL spectra of epitaxial films B21 (right scale) and B22 (left scale) before and after polishing. The spectra are normalized to unity with respect to the amplitude of the 1st order Raman peak at a wavelength of 573 nm. Laser excitation at a wavelength of 532 nm was used.

The synthesized diamond films were boiled in a solution of potassium bichromate in concentrated sulphuric acid for 1 h to remove amorphous carbon that could be deposited on samples in the process of their cooling after the plasma was switched off. After that, they were rinsed with distilled water, boiled in deionized water, and treated with isopropyl alcohol in an ultrasonic bath. One sample (B23) was ground and polished to the thickness of an epitaxial layer ($60\,\mu\text{m}$; $20\,\mu\text{m}$ were removed).

2. Optical spectroscopy

The phase purity of films and the presence of optically active defects in samples were verified by Raman spectroscopy and photoluminescence (PL) spectroscopy using a Renishaw in Via Reflex spectrometer under laser excitation at a wavelength of 532 nm in the backscattering geometry. The Raman spectrum of sample B21 is presented in Fig. 1, *a*. This spectrum contains a single line characteristic of diamond with its maximum at a frequency of $1332.5\,\text{cm}^{-1}$. Its full width at half maximum (FWHM) characterizes primarily the structural perfection of the material and elastic stresses due to the presence of dislocations and other extended defects. The FWHM was 2.2, 2.4, 2.7, and $2.3\,\text{cm}^{-1}$ for films B21, B22, B23, and H03, respectively.

Following the measurements in which films were used as detectors (see Section 3 below), contacts were removed chemically from epitaxial films B21 and B22, and the end face of B21 and the growth surface of B22 were polished. Their PL spectra before and after polishing (for film B21, they were measured at a distance of $5\,\mu\text{m}$ from the growth surface) are shown in Fig. 1, *b*. In addition to the 1st and 2nd order Raman components, these spectra feature two optical centers formed by NV defects (a single substituting nitrogen atom near a carbon vacancy): NV^0 (neutral) and

NV^- (negatively charged) with zero-phonon lines at 575 and 638 nm, respectively, and their phonon repetitions. Since the Fermi level concept is not entirely applicable to wide-bandgap semiconductors with light doping, the same defects are found in several charge states in diamond [34]. The charge state of an NV defect is governed primarily by its local environment [35]. An N_s^0 atom located in the vicinity may transfer its fifth electron to it and form an NV^- optical center that is dominant in the PL spectrum in Fig.1, *b*) (the N_s^0 atom itself then becomes positively charged: N_s^+). It was demonstrated in [36] that the population of NV^- centers in a PL study under excitation in a wavelength range of $450-610\,\text{nm}$ may not exceed 75%. However, the spectra in Fig. 1 are indicative of the presence of N_s^0 atoms in the epitaxial material that do not manifest themselves in luminescence, but affect the charge state of luminescent NV defects.

It can be seen from Fig. 1, *b* that the PL intensities of films B21 and B22 (with respect to the 1st order Raman peak) differ several-fold. Apparently, this is associated with the difference in growth morphology and the corresponding difference in probability of incorporation of nitrogen radicals in the process of film growth. The PL intensity of films B21, B22, and B23 is correlated with FWHM: it is maximized for film B23 (the corresponding FWHM is $2.7\,\text{cm}^{-1}$) and minimized for film B21 (the FWHM is $2.2\,\text{cm}^{-1}$). Notably, the PL intensity of films B21 and B22 decreases considerably after polishing (Fig. 1, *b*). This contradicts the observations made in [37], where the polishing of diamond was found to intensify the luminescence of defects. It is possible that this depends on the polishing mode. In the case of accurate polishing in the soft direction, only plastic flow occurs in the near-surface layer; in the contrary case, defects (specifically, such point defects as vacancies that have the capacity to react with N_s and form NV
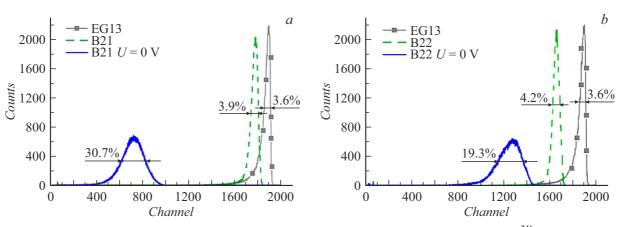
Figure 2. Amplitude spectra of detectors based on samples B21 (*a*) and B22 (*b*) under alpha irradiation from ^{241}Am in comparison with the reference Eg13 (grey) spectrum at (dashed curve) detector voltage $U = -60$ V (on the substrate side) and with (blue curve in the online version of the paper) zero supply voltage $U = 0$ V.

defects [38]) are generated in the process of treatment with brittle removal of material.

Single substituting nitrogen is observed in optical absorption. Absorption at electron transitions in crystals type Ib starts from a quanta energy of 1.7 eV and intensifies smoothly up to the fundamental edge. At low concentrations N_s, the absorption band with a maximum near 270 nm and a FWHM of about 20 nm manifests itself against this background. Its intensity is proportional to concentration N_s^0 [39]. However, it was hypothesized that this band in a material with nitrogen in the form of dominant N_s^0 is associated with the production of negatively charged N_s^- in reaction $N_s^0 + h\nu \to N_s^- + h^+$, where h^+ is a hole in the valence band [40]. Either way, optical absorption in this band is commonly used to determine the concentration of N_s^0 in diamond.

Optical absorption before and after epitaxy was measured in transparent sample H03 in the wavelength range of $230-350$ nm using a LAMBDA 850+ (PerkinElmer, United States) spectrophotometer with a 4 mm aperture. The actual maximum of the peak in our measurement was located at $272-275$ nm. Based on the calibration from [40], the average concentration of N_s^0 in substrate H03 is 95 ± 8 ppb (1 ppb = $1.76 \cdot 10^{14}$ cm^{-3}). The peak with its maximum around 270 nm was not found to intensify after epitaxy. If we factor in the measurement sensitivity and other errors, it is fair to say that the concentration of N_s^0 in epitaxial film H03 with a thickness of $51 \pm 11 \, \mu$m and in films B21$-$B23 synthesized in similar conditions is, in any scenario, below 50 ppb.

3. Efficiency of charge collection in films

Solid metallic platinum contacts with a thickness of 35 nm were deposited by magnetron sputtering at a sample temperature of 250°C onto the growth side of the film and the free side of the conducting substrate in order to measure the efficiency of collection of charges (electrons and holes) produced in diamond by high-energy particles. The sensing

element with deposited contacts was mounted in a special case.

The amplitude spectra of the detector were measured under irradiation with alpha particles from a reference ^{241}Am source with an energy of ~ 5.5 MeV and an activity of ~ 30 kBq under atmospheric pressure (with the detector positioned at a distance of ~ 2 mm from the source) and under irradiation with neutrons from an ING-07T generator. Losses inside the reference source of alpha particles are low, since it is not covered with a protective layer and the active layer is very thin. According to our estimates, the deviation from the theoretical value of energy of a ^{241}Am alpha particle does not exceed 50 keV. Losses at the detector contacts are insignificant (no higher than 2 keV), and the broadening of the peak of the energy spectrum at contacts is below 0.1%. An air gap of 2 mm between the source of alpha particles and the detector induces a ~ 200 keV loss of energy of alpha particles, and the peak broadens by a factor of 3.9. This was measured using a Eg13 detector (which serves as the reference for the presented results), but within a different measurement section. The accelerating voltage of ING-07T was 130 kV at a current of 100 mA. Detectors were positioned at a distance of 5 cm from the neutron generator target along the axis of the accelerated deuterium–tritium generator beam within a flux of neutrons with an energy of ~ 14.7 MeV and a density of $\sim 1.1 \cdot 10^6$ cm$^{-2}s^{-1}$. The measurement section included a Canberra 2004 charge-sensitive preamplifier, an Ortec 673 shaping amplifier, an Ortec 556 power supply, and an Ortec 926 spectrometric ADC.

The measured amplitude spectra were compared with the spectra of a reference diamond Eg13 detector (produced at Project Center ITER from CVD diamond provided by Element Six). Its charge collection efficiency is $\sim 98\%$, and the energy resolution is $\Delta E/E \sim 0.8\%$. The amplitude spectra of detectors based on films B21, B22 within a flux of alpha particles from the ^{241}Am source are presented in Fig. 2, *a*. The corresponding spectra for film B23 are shown in Fig. 3. The measured FWHM values of amplitude peaks

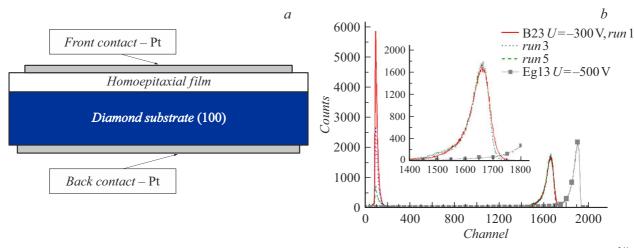**Figure 3.** Schematic diagram of the detector structure (a); b — amplitude spectra of detector B23 under alpha irradiation from ^{241}Am in three measurements (out of five consecutive ones) with bias voltage $U = -300$ V (shown in different colors on the right). The reference Eg13 spectrum (grey) was measured with bias voltage $U = -500$ V. The inset presents the spectra of detector B23 in a narrow energy range. The time of measurement of a single spectrum was $t = 300$ s.

Table 2. Charge collection efficiency ε and widths of Raman peaks of the diamond film ($\Delta\nu_f$) and the substrate ($\Delta\nu_s$)

Sample number	Charge collection efficiency ε, %	Raman peak width of the diamond film $\Delta\nu_f$, cm^{-1}	Raman peak width of the substrate $\Delta\nu_s$, cm^{-1}
Eg13	98	2.2	n/a
B21	92	2.2	3.8
B22	86	2.4	4.0
B23	86	2.7	5.7

of films B21, B22, and B23 were 3.9, 4.2, and 4.24%, respectively, and were governed by the energy spectrum of alpha particles after propagation through ~ 2 mm of air and the energy resolution of the corresponding film. The indicated values are close to the FWHM of the reference Eg13 crystal (3.6%). The FWHM of the energy spectrum of the alpha-particle source for our detectors may be estimated based on the results of measurements for Eg13 in the following way: $\left((3.6\%)^2 - (0.8\%)^2\right)^{0.5} = 3.4\%$. The energy resolutions of films B21–B23 may be estimated accordingly by quadratic subtraction of the width of the energy distribution of alpha particles (3.4%) from the width of their amplitude spectra. This procedure yields the values of 1.7, 2.45, 2.5% for B21–B23, respectively. Note that the path length of alpha particles in diamond is around 12 μm; therefore, electron–hole pairs were generated only in the anode region of the detector volume.

The key difference between the characteristics (e.g., charge collection efficiency) of the reference Eg13 diamond detector, which was produced based on CVD diamond provided by Element Six, and samples B21–B23 examined in the present study is in the concentration of nitrogen in CVD diamond. Element Six states that the concentration of nitrogen in its electronic-grade diamond is on the order of 1 ppb, while it was demonstrated experimentally for our samples that the concentration of nitrogen in them is no higher than 50 ppb, which is sufficient to rate the film material as a detector-grade one. It should be noted that while the Eg13 crystal (chosen as the reference one) is characterized by a low concentration of impurity nitrogen and a high degree of crystalline perfection, its characteristics as an electronic-grade material are not record-high. Therefore, the results obtained with the Eg13 detector differ from literature data for the best samples.

The maximum signal for the reference Eg13 detector corresponded to channel #1899. The efficiency of charge collection in films B21 and B22 determined based on the shift of the peak in the amplitude spectrum upon generation of electron-hole pairs in the anode film region at a bias voltage of 60 V were 92 and 86%, respectively, with a measurement uncertainty of $\pm 0.2\%$. The efficiency of charge collection in film B23 was 86% at a bias voltage of 300 V. The shape stability of the amplitude spectrum should be noted; specifically, the spectra in a series of five consecutive intervals (each having a length of 300 s) for B23 were almost identical. This is indicative of a relatively low density of charge trapping sites in films (the spectra of three measurements out of five consecutive ones are shown in Fig. 3). The WiRE 5.1 software supplied with
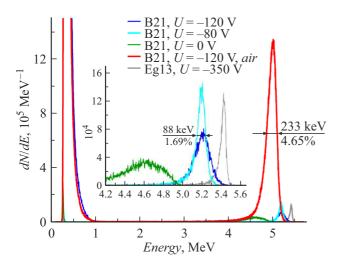
Figure 4. Amplitude spectra of the newly fabricated detector with film B21 within a flux of alpha particles from ^{241}Am in vacuum (dark blue, light blue, green (in the online version)) and in air (red (in the online version)) compared to the spectrum of Eg13 in vacuum (grey (in the online version)).

the spectrometer was used to determine the FWHM values in Raman spectra. The line shape was approximated with a Voigt distribution. Six points were positioned on a Raman line profile. The mean-square deviation of the calculated FWHM values was $0.1\,\mathrm{cm}^{-1}$. It should be noted that the FWHM values of the obtained spectra are somewhat overstated. For example, the FWHM of the neon line of a calibration neon lamp supplied with the instrument was $1.3\,\mathrm{cm}^{-1}$. However, the characteristics of synthesized diamond films presented in Table 2 and Fig. 1 still allow one to state that the charge collection efficiency increases as the Raman peak becomes narrower.

Although the substrates doped with boron did not differ radically in the concentration of boron, which was on the order of 100 ppm, they differed substantially in Raman peak width $\Delta\nu s$. Thus, the substrates had different degrees of

imperfection. According to the data from Table 2, Raman peak width $\Delta\nu_f$ of the film increases with $\Delta\nu_s$; i.e., the film does (to a certain extent) inherit the substrate imperfection. Notably, the best sample B21 corresponds to the substrate with the narrowest Raman peak. The similarity between the Raman peak widths of sample B21 and detector Eg13 from Element Six also indicates that B21 is of a higher quality than samples B22 and B23.

It should be noted that the PL intensity of films B21 and B22 (with respect to the 1st order Raman peak) in the $600-800$ nm range (Fig. 1), which is associated with the presence of nitrogen-vacancy complexes, is also correlated with the charge collection efficiency: the highest efficiency corresponds to sample B21 that has the minimum photoluminescence intensity.

The charge collection efficiency depends to a considerable extent on impurities and point defects that act as traps and carrier scattering sites.

In order to estimate the influence of contacts on CCE and the energy resolution of the detector, platinum contacts of sample B21 were removed chemically and deposited once again. The sample with film B21 with newly fabricated 35-nm-thick platinum contacts was again mounted in a detector case, and its amplitude spectra within fluxes of alpha particles of the same ^{241}Am source were measured in air and in vacuum (at a source–detector distance of 2 and 20 mm, respectively) in the conditions similar to those set in previous measurements. The measured amplitude spectra of B21 with new contacts (see Fig. 4) revealed a CCE of $\sim 94\%$ and an energy resolution of 88 keV (1.69%).

The amplitude spectra of detectors with films B21, B22, and B23 within fluxes of neutrons with an energy of 14.7 MeV and a FWHM of the energy distribution of ~ 320 keV were measured in order to obtain a lower-bound estimate of the charge collection efficiency upon uniform generation of electron–hole pair within the entire volume of synthesized diamond films. The obtained amplitude spectra, which are shaped by reactions $C(n,n)C$, $C(n,\alpha)2\alpha$, and $C(n,\alpha)Be$ [13] (Fig. 5), revealed a high efficiency of charge
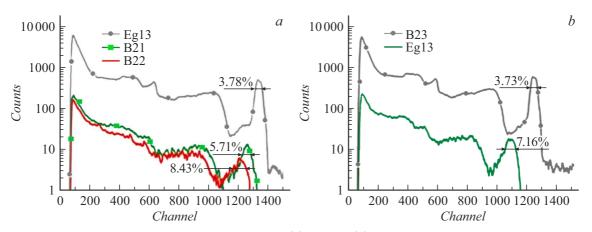

Figure 5. Amplitude spectra of detectors with films B21 and B22 (*a*) and B23 (*b*) within a flux of neutrons with an energy of 14.7 MeV from the ING-07T generator at a distance of 5 cm from its target.

collection in the synthesized B21, B22, and B23 films in the case of generation of electron–hole pairs distributed uniformly throughout the volume. The measured shifts of the peak associated with reaction $C(n, \alpha)Be$ (right peaks in Fig. 5) in the amplitude spectrum provided an opportunity to obtain lower-bound estimates of the efficiency of charge collection in B21, B22, and B23: 91, 85, and 85%, respectively. The considerable enhancement of width of $C(n, \alpha)Be$ peaks (Fig. 5) relative both to the reference Eg13 and to the spectra within fluxes of alpha particles (Figs. 2−4) may be attributed both to a significantly lower measurement statistics and to the fact that an appreciable fraction of charged products of reaction $C(n, \alpha)Be$ produced near the substrate–film interface in thin films may leave the film without transferring all of their energy.

Conclusion

Homoepitaxial undoped detector-grade diamond films with a thickness up to $80\,\mu m$ were synthesized in a modernized microwave plasmachemical reactor in CH_4/H_2 mixtures on single-crystalline diamond substrates doped with boron. It was demonstrated that the charge collection efficiency increases as the width of the diamond line in the Raman spectrum of a film decreases (the degree of crystalline perfection grows) and the PL intensity goes down. It was proven experimentally that the efficiency of collection of charges produced in synthesized diamond by fluxes of alpha particles with an energy of 5.5 MeV and neutrons with an energy 14.7 MeV is as high as 94 and 91%, respectively. Radiation detectors constructed based on diamond films featured a high stability of parameters in detection of alpha particles and neutrons.

Although the synthesized films are photoluminescent due to the presence of nitrogen-vacancy complexes, they demonstrate a high charge collection efficiency and are thus suitable for detector applications.

Conflict of interest

The authors declare that they have no conflict of interest.

References

[1] A. Alekseyev, G. Martin. Nucl. Instrum. Methods Phys. Res., **A 417**, 400 (1998). DOI: 10.1016/S0168-9002(98)00762-1

[2] H. Frais-Kolbl, E. Griesmayer, H. Kagan, H. Pernegger. IEEE Transactions Nucl. Sci., **NS-51**, 3833 (2004). DOI: 10.1109/TNS.2004.839366

[3] H. Kagan. Nucl. Instrum. Methods Phys. Res., **A 541**, 221 (2005). DOI: 10.1016/j.nima.2005.01.060

[4] M. Bruzzi, S. Miglio, S. Pirollo, S. Sciortino. Diamond and Related Mater., **10** (3−7), 601 (2001).

[5] C. Bauer, I. Baumann, C. Colledani, J. Conway, P. Delpierre, F. Djama, M. Zoeller. Nucl. Instrum. Methods Phys. Res. Section A: Accelerators, Spectrometers, Detectors and Associated Equipment, **383** (1), 64 (1996).

[6] E.A. Konorova, S.F. Kozlov. Sov. Phys. Semicond, **4**, 1600 (1971).

[7] A.V. Krasilnikov, E.A. Azizov, A.L. Roquemore, V.S. Khrunov, K.M. Young. Rev. Sci. Instrum., **68** (1), 553 (1997).

[8] A.V. Krasilnikov, V.N. Amosov, P. van Belle, O.N. Jarvis, G.J. Sadler, Nucl. Instrum. Meth. Phys. Res., **A 476** (1), 516 (2002).

[9] M. Marinelli, E. Milani, G. Prestopino, A. Tucciarone, C. Verona, G. Verona-Rinati, M. Angelone, D. Lattanzi, M. Pillon, R. Rosa, E. Santoro. Appl. Phys. Lett., **90**, 183509 (2007).

[10] R.S. Balmer, J.R. Brandon, S.L. Clewes, H.K. Dhillon, J.M. Dodson, I. Friel, P.N. Inglis, T.D. Madgwick, M.L. Markham, T.P. Mollart, N. Perkins, G.A. Scarsbrook, D.J. Twitchen, A.J. Whitehead, J.J. Wilman, S.M. Woollard. J. Phys.: Condens. Matter, **21**, 364221 (2009).

[11] M. Pillon, M. Angelone, A. Krasa, A.J.M. Plompen, P. Schille-beeckx, M.L. Sergi. Nucl. Instrum. Meth. Phys. Res., **A 640**, 185 (2011).

[12] P. Barberet, M. Pomorski, G. Muggiolu, E. Torfeh, G. Claverie, C. Huss, S. Saada, G. Deves, M. Simon, H. Seznec. Appl. Phys. Lett., **111**, 243701 (2017).

[13] H. Kagan, A. Alexopoulos, M. Artusot, F. Bachmair et al. Nucl. Instrum. Meth. Phys. Res., **A 924**, 297 (2019).

[14] C.Y. Lee, C.M. Ban, H.R. Lee, K.N. Choo, B.H. Jun. Appl. Rad. Isotopes, **152**, 25 (2019).

[15] A.V. Krasilnikov. Issues Atom. Sci. Tech., **36** (1), (1995).

[16] A. Tallaire, J. Achard, F. Silva, O. Brinza, A. Gicquel. Comptes Rend. Phys., **14**, 169 (2013). https://doi.org/10.1016/j.crhy.2012.10.008

[17] S. Nad, Y. Gu, J. Asmussen. Diam. Relat. Mater., **60**, 26 (2015).

[18] A.P. Bolshakov, V.G. Ralchenko, V.Y. Yurov, A.F. Popovich, I.A. Antonova, A.A. Khomich, E.E. Ashkinazi, S.G. Ryzhkov, A.V. Vlasov, A.V. Khomich. Diam. Relat. Mater., **62**, 49 (2016).

[19] A.L. Vikharev, M.A. Lobaev, A.M. Gorbachev, D.B. Radishev, V.A. Isaev, S.A. Bogdanov. Mater. Today Comm., **22**, 100816 (2020).

[20] Z. Minglong, X.Yiben, W. Linjun, S. Hujiang, G. Beibei. Solid State Commun., **130**, 551 (2004).

[21] F. Schirru, D. Chokheli, M. Kis. Diam. Relat. Mater., **49**, 96 (2014).

[22] A. Balducci, M. Marinelli, E. Milani, M.E. Morgada, G. Pucella, M. Scoccia, A. Tucciarone, G. Verona-Rinati, M. Angelone, M. Pillon, R. Potenza, C. Tuve. Diam. Relat. Mater., **15**, 292 (2006).

[23] M. Pomorski, C. Delfaure, N. Vaissiere, H. Bensalah, J. Barjon, M.A. Pinault-Thaury, D. Tromson, P. Bergonzo. Phys. Stat. Sol. A, **212** (11), 2553 (2015). DOI: 10.1002/pssa.201532230

[24] T. Shimaoka, J.H. Kankeko, M. Tsubota, H. Shimmyo, H. Watanabe, A. Chayahara, H. Umezawa, S. Shikata. Europhys. Lett., **113** (6), 62001 (2016).

[25] S.V. Chernykh, S.A. Tarelkin, A.V. Chernykh, S.Yu. Troschiev, N.V. Luparev, N.V. Kornilov, D.V. Teteruk, S.A. Terentiev, V.D. Blank, A.V. Antipov, A.P. Chubenko, Yu.N. Glybin, N.I. Polushin, S.I. Didenko. Instrum. Exp. Tech. **62** (4), 473 (2019).

[26] N.B. Rodionov, A.F. Pal', A.P. Bol'shakov, V.G. Ral'chenko, R.A. Khmel'nitskiy, V.A. Dravin, S.A. Malykhin, I.V. Altukhov, M.S. Kagan, S.K. Paprotskiy. J. Commun. Technol. Electron. **63** (7), 828 (2018).

[27] S. Almaviva, M. Marinelli, E. Milani, G. Prestopino, A. Tucciarone, C. Verona, G. Verona-Rinati, M. Angelone, M. Pillon. Nucl. Instrum. Meth. Phys. Res., **A 612**, 580 (2010).

[28] N.B. Rodionov, V.N. Amosov, K.K. Artem'ev, S.A. Meshchaninov, V.P. Rodionova, R.A. Khmel'nitskii, V.A. Dravin, A.P. Bol'shakov, V.G. Ral'chenko. At. Energy, **121** (2), 127 (2016).

[29] N.B. Rodionov, V.N. Amosov, S.A. Meshchaninov, A.F. Pal', V.P. Rodionova, A.G. Trapeznikov. Instrum. Exp. Tech., **59**, 698 (2016).

[30] A.P. Bolshakov, V.G. Ralchenko, G. Shu, B. Dai, V.Yu. Yurov, E.V. Bushuev, A.A. Khomich, A.S. Altakhov, E.E. Ashkinazi, I.A. Antonova, A.V. Vlasov, Y.Y. Sizov, S.K. Vartapetov, V.I. Konov, J. Zhu. Mater. Today Commun., **25**, 101635 (2020). DOI: 10.1016/j.mtcomm.2020.101635

[31] R. Samlenski, C. Haug, R. Brenn, C. Wild, R. Locher, P. Koidl. Appl. Phys. Lett., **67**, 2798 (1995).

[32] M.N.R. Ashfold, J.P. Goss, B.L. Green, P.W. May, M.E. Newton, C.V. Peaker. Nitrogen Diamond. Chem. Rev., **120** (12), 5745 (2020).

[33] A. Tallaire, M. Kasu, K. Ueda, T. Makimoto. Diam. Relat. Mater., **17** (1), 60 (2008).

[34] A.T. Collins. J. Phys.: Condens. Matter., **14**, 3743 (2002).

[35] J.P. Goss, P.R. Briddon, R. Jones, S. Sque. Diam. Relat. Mater., **13**, 684 (2004).

[36] N. Aslam, G. Waldherr, P. Neumann, F. Jelezko, J. Wrachtrup. New J. Phys., **15**, 013064 (2013).

[37] P.-N. Volpe, P. Muret, F. Omnes, J. Achard, F. Silva, O. Brinza, A. Gicquel. Diam. Relat. Mater., **18**, 1205 (2009).

[38] H. Luo, K.M. Ajmal, W. Liu, K. Yamamura, H. Deng. Int. J. Extrem. Manuf., **3**, 022003 (2021).

[39] H.B. Dyer, F.A. Raal, L. DuPreez, J.H.N. Loubser. Philos. Mag., **11**, 763 (1965).

[40] R. Jones, J.P. Goss, P.R. Briddon. Phys. Rev. B: Condens. Matter. Mater. Phys., **80**, 033205 (2009).